Journal of Materials Chemistry A

PAPER

View Article Online
View Journal | View Issue

Cite this: J. Mater. Chem. A, 2014, 2, 12340

3D conductive network-based free-standing PANI–RGO–MWNTs hybrid film for high-performance flexible supercapacitor

Haosen Fan,[ab] Ning Zhao,*[b] Hao Wang,[b] Jian Xu*[b] and Feng Pan*[a]

Received 29th April 2014
Accepted 2nd June 2014

DOI: 10.1039/c4ta02118e

www.rsc.org/MaterialsA

A facile method was successfully established to construct 3D conductive network-based free-standing polyaniline/reduced graphene oxide/carbon nanotube ternary hybrid film, in which a 3D conductive network was synergistically assembled by MWNTs and GO. The synergistic assembly of carbon nanotubes and graphene oxide not only increased the basal spacing between graphene sheets but also effectively bridged the defects of reduced graphene oxide to form a 3D conductive network. Due to the 3D conductive network with high conductivity and the synergistic effect of polyaniline with carbon nanotubes and graphene, the as-prepared ternary hybrid film possessed high specific capacitance and good cycle stability as a flexible supercapacitor electrode. This study gives a better insight for the preparation of functional flexible hybrid film by combining conducting polymer with carbon materials of different dimensions.

Introduction

With growing concerns over finite fossil-fuel supplies and environmental issues, the development of alternative energy conversion/storage resources is very important and indispensable.[1] Supercapacitors, also called electrochemical capacitors, are likely to play an important role in energy storage due to their high power density, long cycle life and many potential applications in portable electronic devices, hybrid electric vehicles and implantable medical devices.[2,3] Recently, there has been increasing interest in flexible supercapacitors as energy storage devices to meet the various requirements of modern applications.[4,5] An ideal flexible supercapacitor should have a combination of good flexibility with excellent mechanical strength and large electrochemical behavior.[6] Although conducting polymers and transition metal oxides have been widely studied as supercapacitors due to their prominent capacitive properties, only carbon materials (carbon fibers,[7,8] carbon nanotubes[9,10] and graphene[11,12]) have displayed favorable flexibility; hence, they have been promising as free-standing and flexible capacitors.

Recently, graphene sheet, a two-dimensional all-sp^2-hybridized carbon, has been proposed as one of the ideal candidates for next-generation flexible electrode materials, not only due to its structural, mechanical and electrical properties, but also due to its high accessible surface area (2630 m^2 g^{-1}).[13] In general, graphene or graphene oxide sheets are often combined with polyaniline (PANI) to improve the capacitance property of flexible films because of the special synergistic effect of PANI and graphene or graphene oxide sheets. It is well known that PANI is one of the most promising conducting polymers that shows high capacitance, has good environmental stability and is easy to prepare. PANI materials have been widely studied to promote the electrochemical capacitance of flexible CNT and graphene papers.[14,15] However, previous reports indicate that the actual performance of graphene-based materials is much lower than the anticipated value (estimated from the ultra-high surface area of graphene) due to the facile aggregation of graphene during preparation, attributing to facile restacking of reduced graphene oxide because of strong van der Waals interactions between individual graphene sheets.[16] Fortunately, the combination of carbon nanotubes and graphene has been demonstrated to improve the capacitance property of graphene with the existence of carbon nanotubes, which are believed to increase the basal spacing between graphene sheets, as well as to bridge the defects of graphene for fast electron transfer.[17–19] Therefore, the inclusion of carbon nanotubes is expected to improve the unique potential of graphene film as a free-standing electrode for supercapacitors.

Herein, we demonstrate the preparation of a hierarchical flexible polyaniline/reduced graphene oxide/carbon nanotube ternary film, based on a 3D conductive network, by introducing carbon nanotubes into the graphene system. This film is prepared by a rapid-mixture polymerization of aniline monomers in the presence of flexible graphene oxide/carbon

[a]School of Advanced Materials, Peking University Shenzhen Graduate School, Shenzhen 518055, P.R. China. E-mail: panfeng@pkusz.edu.cn; Fax: +86-755-26033200; Tel: +86-755-26033200

[b]Beijing National Laboratory for Molecular Sciences, Laboratory of Polymer Physics and Chemistry, Institute of Chemistry, Chinese Academy of Sciences, Beijing 100190, P.R. China. E-mail: zhaoning@iccas.ac.cn; jxu@iccas.ac.cn

nanotube composite film. This novel flexible film exhibits excellent electrochemical performance due to the high electrical conductivity of the 3D conductive network and extraordinary architecture, which can effectively combine both the faradaic capacitance and double-layer capacitance at the electrode–electrolyte interfaces. The as-prepared ternary flexible film shows high specific capacitance in 1 M H_2SO_4 aqueous solution, showing its promising application in flexible supercapacitors.

Experimental

Materials

Aniline (ANI, Beijing Chemical Co.) was distilled under reduced pressure. Ammonium persulfate (APS, Sinopharm Chemical Reagent Co.), graphite (Alfa Aesar, 325 mesh), commercial multiwall carbon nanotubes (MWNTs, 10–30 nm in diameter, 5–15 μm in length, purity ≥ 95 wt%, Shenzhen Nanotech Port Co., Ltd.), and other reagents were all of A. R. grade and used without further treatment.

Preparation of PANI–RGO–MWNTs hybrid film

Firstly, 50 mg graphene oxide (GO, prepared by the modified Hummers method[20]) was dispersed in distilled water (50 mL) by ultrasonic treatment for 30 min. MWNTs (50 mg) were added, and then sonicated for another 30 min. The resultant complex dispersion was filtered by a vacuum filter equipped with a 0.45 μm porous PTFE membrane to produce a MWNTs–GO film. Secondly, PANI and MWNTs–GO hybrid film were synthesized by a typical rapid-mixture polymerization. Aniline (1 mmol) was dissolved in 50 mL of 1 M $HClO_4$ solution, and APS (1 mmol) was dissolved in 20 mL of the same $HClO_4$ solution. The two solutions were then rapidly poured together and immediately stirred to ensure sufficient mixing before the polymerization began. After being stirred vigorously for 1 min, the stirring was stopped, and the MWNTs–GO film was carefully immersed into it. Note that reactions were carried out at room temperature for 12 h without stirring. The obtained PANI–GO–MWNTs film was rinsed several times with distilled water. Finally, the PANI–GO–MWNTs film was reduced by 55% hydroiodic acid for 1 h at 100 °C,[21] and the final PANI–RGO–MWNTs ternary composite film was obtained.

Electrochemical measurements

Electrochemical performances of all samples were measured with a three-electrode system, in which platinum foil and saturated calomel electrode (SCE) were used as counter and reference electrodes, respectively. The electrolyte is 1 M H_2SO_4 aqueous solution. Cyclic voltammetry (CV) and electrochemical impedance spectroscopy (EIS) measurements were performed by using a Zahner IM6 electrochemical working station. The scan voltage ranged from −0.2 to 0.8 V for the CV measurements.

Characterization

The morphology of all products was characterized by scanning electron microscopy (SEM, Hitachi S4800) and transmission electron microscopy (TEM, JEOL JEM-2200FS). Fourier transform infrared (FTIR) spectra were recorded on a Bruker Equinox 55 spectrometer in the range of 400–4000^{-1} cm at room temperature. X-ray photoelectron spectroscopy (XPS) analysis was carried out on an ESCALab220i-XL electron spectrometer from VG Scientific. Al-Kα radiation was used as the X-ray source and operated at 300 W.

Results and discussion

As shown in Fig. 1a, a simple strategy is designed to improve the capacitive performances by introducing MWNTs into GO and then combining with PANI. The GO and MWNTs mixture is first dispersed in aqueous media by ultrasonication, and a GO–MWNTs film is prepared by filtration of the diluted dispersion. In this procedure, the long and tortuous MWNTs, which play an important role in inhibiting the aggregation of 2D GO, are embedded between the GO layers, which will effectively increase the contact surface area with electrolytes. Thus, the incorporation of MWNTs embedded between GO layers will not only provide open channels for ionic transport and reduced ionic diffusion length by preventing the aggregation of graphene but

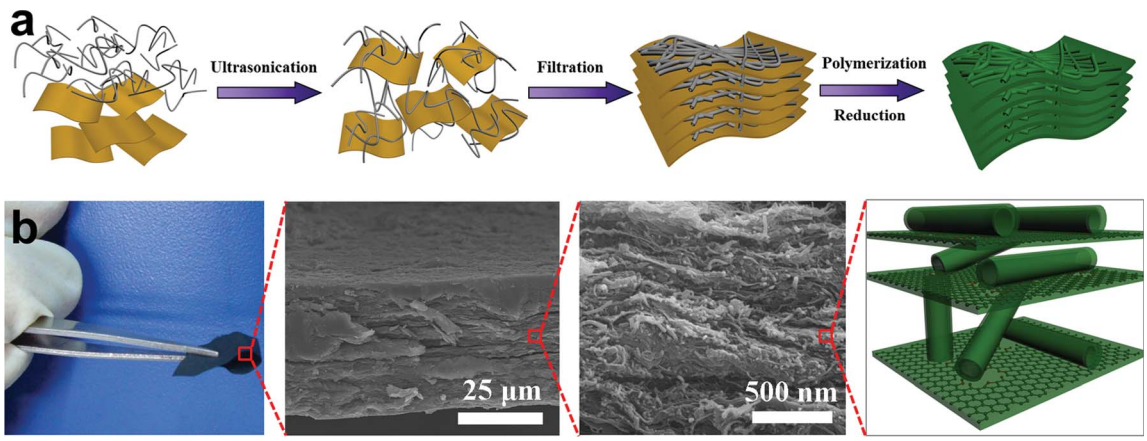

Fig. 1 Schematic illustration of the formation of flexible PANI–RGO–MWNTs ternary hybrid film.

also be able to bridge the gaps between reduced GO to form a three-dimensional conductive network, which provides efficiently conductive pathways for electron conduction in the ternary film. After a rapid-mixture polymerization of aniline in the presence of GO–MWNTs film and reduction of the GO in hydroiodic acid, as shown in Fig. 1b, the final PANI–MWNTs–graphene ternary composite film is successfully prepared with a sandwich-like structure of stacked layers. As a result, owing to a 3D conductive network as the supported skeleton and the synergistic effect of polyaniline with carbon nanotubes and graphene, a ternary flexible electrode material with improved capacitive performance of high specific capacitance can be anticipated by designing hierarchical PANI–RGO–MWNTs architecture.

Fig. 2 shows the aqueous dispersibility of GO, MWNTs and GO–MWNTs. It is well known that GO sheets can be formed as well-dispersed aqueous colloids by ultrasonic dispersion. Unfortunately, GO sheets are still able to aggregate together if they are kept stationary for a day. This is mainly due to facile restacking of GO sheets by van der Waals forces. The MWNTs show poor dispersion because most of the MWNTs are deposited at the bottom after ultrasonication is stopped for 5 minutes. However, the GO–MWNTs dispersion exhibits good dispersibility due to inserting MWNTs into the interlayer of GO sheets. Hence, the purpose of obtaining a mutual dispersion of MWNTs and GO is achieved by the ultrasonic dispersion of their mixture solution. Note that a good GO–MWNTs dispersion liquid can keep for a month in stationary state without any deposition.

It is observed that the filtration of the aqueous GO dispersion through a cellulose membrane filter yielded, after vacuum drying, a brown, free-standing and flexible GO film.

(Fig. 3a). The GO film can be easily rolled up on a glass rod (Inset of 3a). GO–MWNTs film is obtained by the same filtration method, and it also shows flexible properties; however, the color of the film is black, which is different from the color of GO film, with an obvious metallic luster (Fig. 3b and inset). The thickness of the film can be adjusted by changing the concentration

Fig. 2 Digital camera images of the aqueous dispersibility of GO, MWNTs and GO–MWNTs.

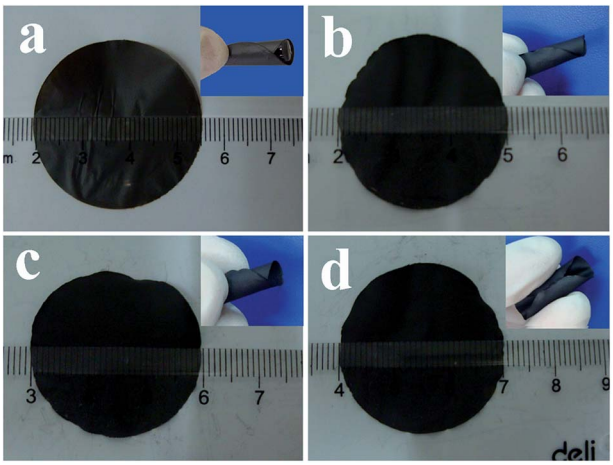

Fig. 3 Digital camera images of flexible films (a) GO, (b) GO–MWNTs, (c) PANI–GO–MWNTs, and (d) PANI–RGO–MWNTs. (The inset images indicate the flexibility of the samples.).

and volume of GO or GO–MWNTs aqueous dispersion. After polymerization, the PANI layer was coated on the surface of GO and embedded between GO–MWNTs layers to generate PANI–GO–MWNTs film, which maintained the original integrity with good flexibility (Fig. 3c, and Insets). The PANI–RGO–MWNTs, which were reduced from PANI–GO–MWNTs, also maintained good flexibility (Fig. 3d and insets). For similarity with GO and GO–MWNTs hybrid films, the PANI–GO/RGO–MWNTs films with controllable thickness can be rolled up or bent easily without cracking, which is surely beneficial to its practical application in flexible electrode materials. Hence, the rapid-mixture polymerization, in which the PANI was grown on the GO surfaces and between GO–MWNTs layers to generate the flexible films, exhibits great advantages of simple and large-area preparation. Moreover, PANI coatings are facilely obtained and controlled with high specific surface area, and they retain the flexibility of the pristine GO–MWNTs film.

Fig. 4a and d show the cross-section and surface SEM images of GO–MWNTs film. The fracture edges of the film image exhibit a layered structure with well-compacted, layer-by-layer alternate stacking of GO and MWNTs in almost the entire cross-section. Note that MWNTs are uniformly sandwiched between the GO sheets. Surface SEM and high-resolution SEM images (Fig. 4d) reveal that the surfaces of the GO–MWNTs film are quite smooth with GO sheets coating on MWNTs. After a rapid-mixture polymerization of aniline and reduction of GO by hydroiodic acid, the cross-section SEM images of PANI–GO–MWNTs (Fig. 4b) and PANI–RGO–MWNTs (Fig. 4c) films illustrate that they still retain the layer-by-layer structure of the GO–MWNTs with the exception of the coating of PANI. As can be seen in the surface images of PANI–GO–MWNTs (Fig. 4e) and PANI–RGO–MWNTs (Fig. 4f) films, they are both sufficiently rough with numerous nanoscale protuberances, indicating the combination of PANI with GO and MWNTs. As is well known, many oxygen-containing functional groups, such as carboxylic and phenolic hydroxyl groups, exist on the surface and edges of GO sheets. In our rapid-mixture polymerization process, after

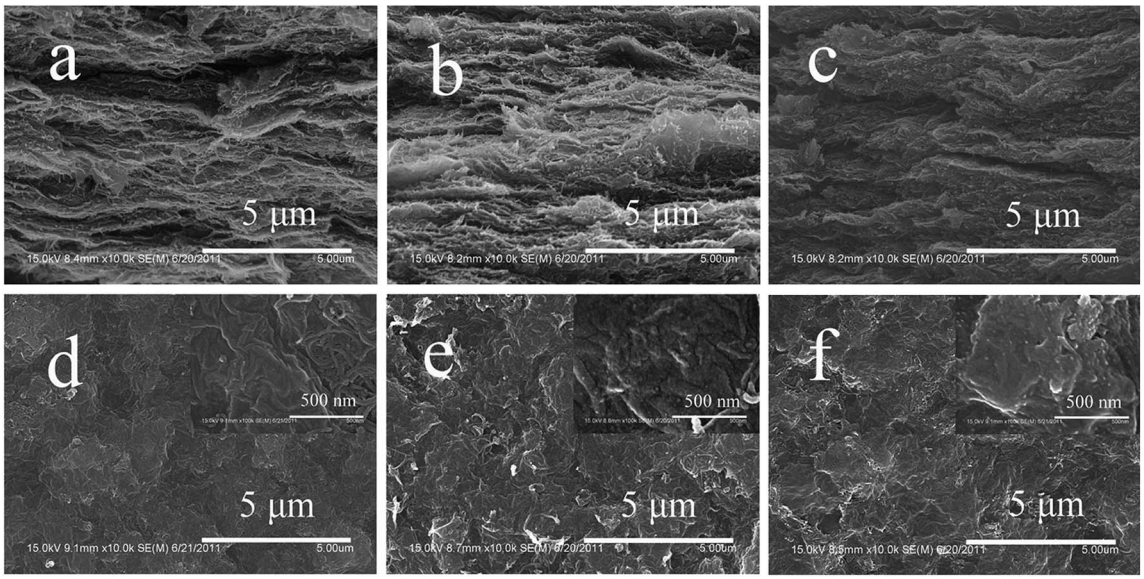

Fig. 4 Cross-section and surface SEM images of GO–MWNTs film (a and d), PANI–GO–MWNTs film (b and e) and PANI–RGO–MWNTs film (c and f). (Insets show high-resolution SEM images of the surface).

immersing the GO–MWNTs film into the reaction system, the functional groups may act as active sites by preferentially adsorbing anilinium ions though electrostatic force. Thus, these sites will act as the seeding dots to attach the polymerization of PANI on the surface of GO and between the GO–MWNTs layers to form PANI nanoparticles and PANI coatings.

Fig. 5 presents TEM images of the broken films by ultrasonic treatment. It is important to note that ultrasonic treatment cannot completely destroy the film into a single-layer GO and MWNTs, but it transforms the film into a close-packed structure. As showed in Fig. 5a and b, it can be found that MWNTs are randomly distributed into the GO sheet by connecting to

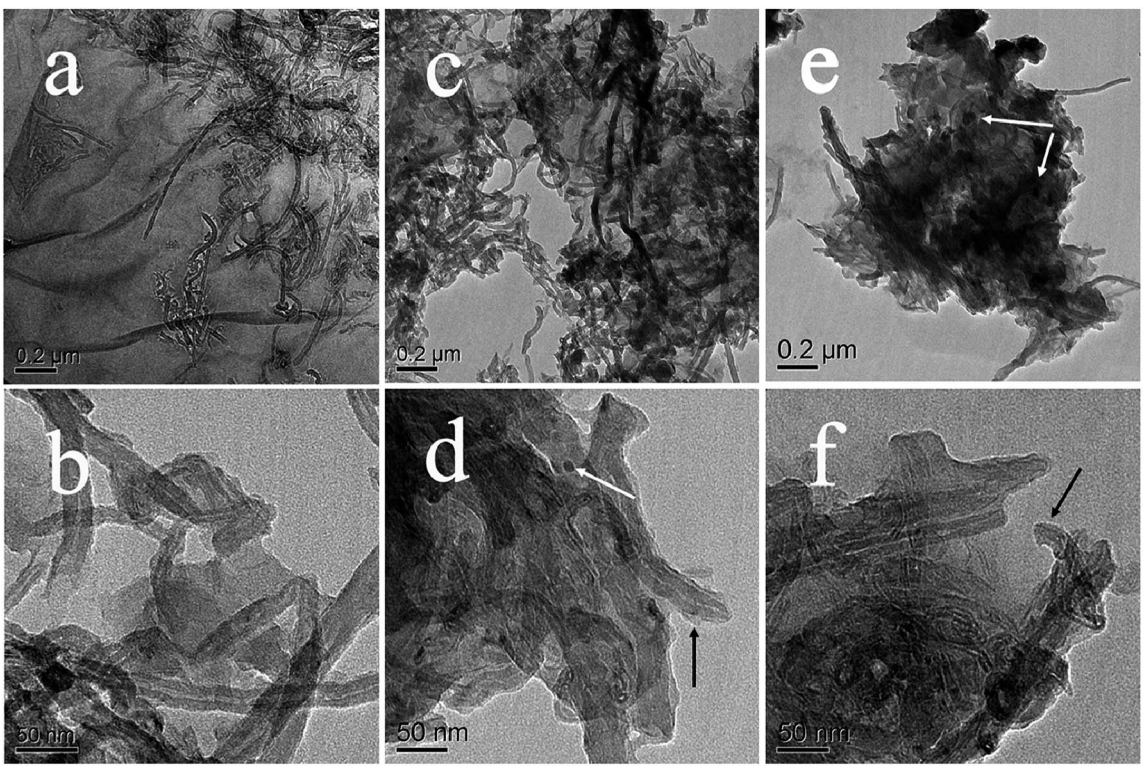

Fig. 5 TEM images of GO–MWNTs film (a and b), PANI–MWNTs–GO film (c and d) and PANI–GRO–MWNTs film (e and f).

each other to form a sandwich-like structure. After polymerization of aniline (Fig. 5c and d), core–shell nanostructures with thin PANI layer coated on MWNTs are formed (black arrow), in addition to PANI nanoparticles on the surface of GO (white arrow). As is well known, MWNTs used here are not treated by inorganic acids. The π–π stacking force between the graphitic structures of MWNTs and the aromatic rings of PANI is conducive to the polymerization PANI layer on the surface of MWNTs. Moreover, except for the PANI nanoparticles formed in the GO oxided site by electrostatic force, the π–π stacking force between PANI and GO also contributes to the PANI layer on the nonoxided parts of GO, providing a sandwich-structured PANI–GO. After the reduction of GO, as shown in Fig. 5e and f, the coaxial structure of PANI–MWNTs and PANI–RGO is retained, indicating that the reduction process retains the same structure in the PANI–RGO–MWNTs film. Here, it is worth noting that ultrasonic treatment also did not fully destroy the ternary hybrid films into a single or few layers of GO and MWNTs, showing the agglomerate structure in the TEM images.

The typical FT-IR spectra of all samples are shown in Fig. 6a. MWNTs show no obvious absorption peak; however, compared to pristine MWNTs, GO–MWNTs show similar characteristic peaks around 3399, 1729 and 1391–1060 cm^{-1}, which can be attributed to the O–H, C=O in COOH, and C–O in C–OH/C–O–C functional groups, respectively.[22] The resultant PANI–RGO–MWNTs film exhibits similar specific peaks as compared to the peaks of pure PANI. The main transmission bands centered at 1566 and 1486 cm^{-1} are attributed to C=C stretching vibrations of quinoid ring and benzenoid ring in PANI chains, indicating the presence of an emeraldine salt state in PANI. The peaks at 1298, 1246, 1146 and 818 cm^{-1} are attributed to the following vibrations: C–N stretching vibration of the benzene ring, stretching vibration of the $CN^{\bullet+}$ in the polaron structure of PANI, stretching of C=N (–N = quinoid = N–) and out-of-plane bending vibrations of C–H in the benzene ring, respectively.[23]

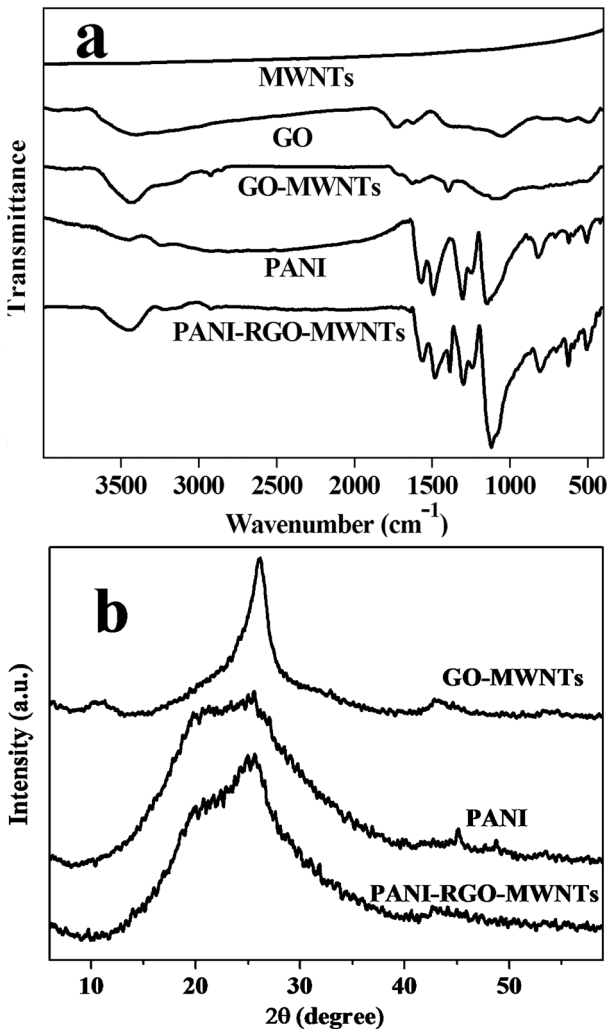

Fig. 6 FTIR and XRD spectra of the obtained examples.

Fig. 6b shows the XRD patterns of GO–MWNTs, GO and PANI–RGO–MWNTs. The typical peaks of GO–MWNTs centered at $2\theta = 26.1^\circ$ correspond to the (002) interplanar spacing between the MWNTs walls.[24] For pure PANI, the crystalline peaks centered at about 20° and 26° can be assigned to (020) and (200) reflections of PANI, suggesting its emeraldine salt form.[25] The XRD patterns of PANI–RGO–MWNTs exhibit similar crystal peaks compared with that of PANI, revealing that no additional crystalline order is introduced into the obtained ternary hybrid film in the presence of RGO and MWNTs.

XPS (Fig. 7a) is used to measure elemental composition on the surface. The survey spectrum shows that GO–MWNTs consist of oxygen (531 eV) and carbon (285 eV). PANI–GO–MWNTs display additional nitrogen groups (399 eV) due to the PANI coating on the surface of GO and MWNTs. After the reduction of PANI–GO–MWNTs, the O element content decreases due to the removal of the oxygen-containing functional group in the GO. In the C 1s spectrum of GO in Fig. 7b, GO shows the highest hetero-carbon with four components that correspond to carbon atoms in different functional groups: the nonoxygenated ring C (284.9 eV), the C atom in C–O bond (286.2 eV), the carbonyl C (287.8 eV), and the carboxylate carbon (O–C=O) (289.0 eV). These functional groups can be effectively removed by HI reduction, which can be confirmed by the significant decrease in the hetero-carbon component in Fig. 7b as compared to Fig. 7c. After HI reduction, although the C1s XPS spectrum of the RGO also exhibits the same oxygen groups as compared to the C1s spectrum of GO, their peak intensities are much smaller than those in GO. The percentage of C=C bond in the composite increases from 53.6% to 82.4%, revealing remarkable restoration of the graphitic structure of RGO through HI reduction. All the above results clearly reveal that GO is successfully reduced to RGO in this simple HI reduction method.

The electrochemical performance of the flexible film samples were characterized by cyclic voltammograms (CV) and electrochemical impedance spectroscopy (EIS). Fig. 8a exhibits the CV curves of all examples at a sweep rate of 5 mV s^{-1} with a potential range from −0.2 to 0.8 V in 1 M H_2SO_4 solution. For PANI–RGO–MWNTs and PANI–GO–MWNTs electrodes, the two couples of redox peaks, *i.e.*, $C_1/A_1$and C_2/A_2, in CV curves result in the redox capacitance. The redox peak C_1/A_1 is attributed to the redox transition of PANI from leucoemeraldine

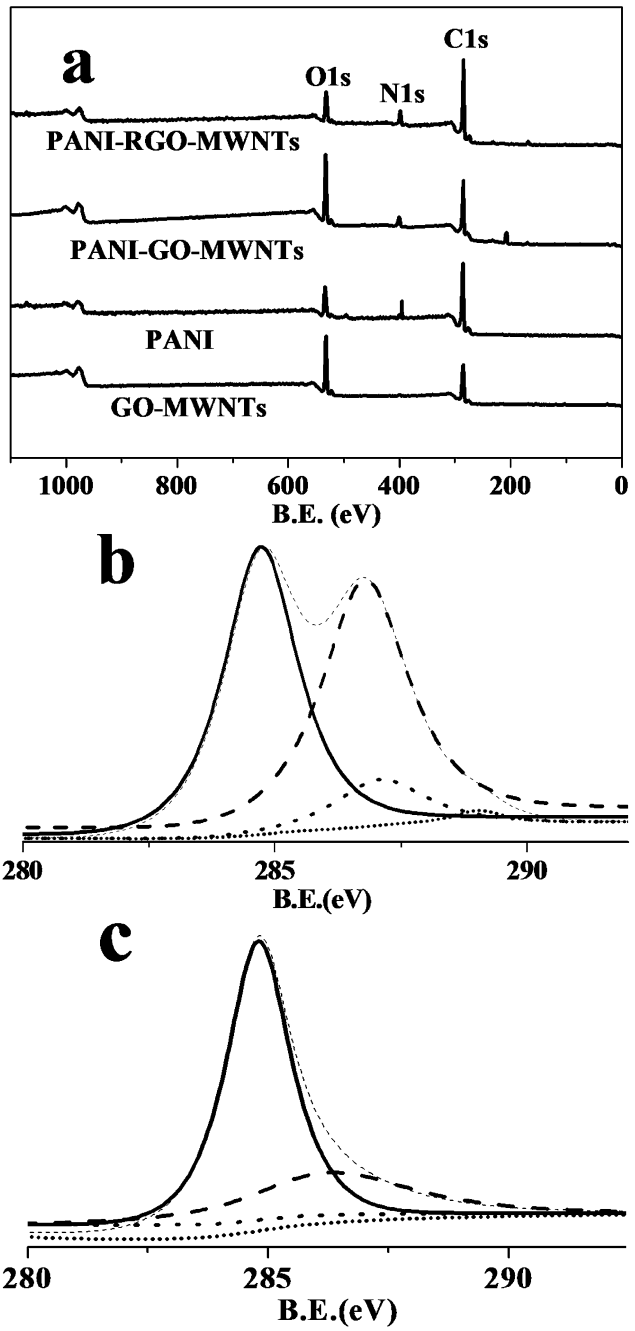

Fig. 7 XPS spectra of all examples (a) C1s spectra of (b) GO and (c) RGO.

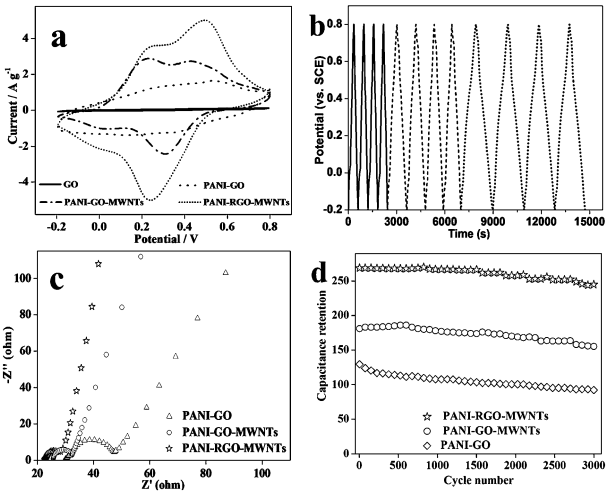

Fig. 8 (a) CV curves of MWNTs, PANI–GO, PANI–GO–MWNTs and PANI–RGO–MWNTs. (b) Continuous galvanostatic charge–discharge curves of PANI–RGO–MWNTs electrode at the current densities of 2 A g^{-1}, 1 A g^{-1} and 0.5 A g^{-1}. (c) Electrochemical impedance spectroscopy of the three electrodes. (d) Variation of the specific capacitance of three samples *versus* the cycle number.

(semiconducting state) to emeraldine form (conducting state), whereas C_2/A_2 is ascribed to the transformation from emeraldine to pernigraniline.[25,26] PANI–RGO–MWNTs ternary film exhibits a larger current density response compared to GO, PANI–GO and PANI–GO–MWNTs electrodes at the same scan rate, suggesting that the ternary hybrid film has higher specific capacitance.

The galvanostatic charge/discharges of the PANI–RGO–MWNTs film electrode at different current densities were measured in 1 M H_2SO_4. As shown in Fig. 8b, the charge–discharge curves at each four continuous cycles have a similar shape, which indicates that the ternary film can experience a wide range of current densities. PANI–RGO–MWNTs film electrode exhibits a high discharge/charge efficiency of 98.7%, according to the ratio of the discharge time to the charge time, indicating excellent electrochemical reversibility and discharge/charge rate control capability. The specific capacitance of the electrode can be calculated from CV curves, according to the equation, $C_m = (I\Delta t)/(\Delta Vm)$, where C_m is the specific capacitance, I is the constant discharge current, Δt is the discharge time, ΔV is the potential window, and m is the mass of the electroactive materials.[27] The specific capacitance of the PANI–RGO–MWNTs is about 498 F g^{-1} at 0.5 A g^{-1}. The greatly enhanced specific capacitance may result from the synergistic effect between RGO, MWNTs and PANI, in addition to the good electrical conductivity of the 3D conductive network synergistically assembled by MWNTs and RGO.

Fig. 8c exhibits the Nyquist diagrams of all examples, which all consist of a semicircle in the high-frequency region and a straight line in the low-frequency region, corresponding to the charge-transfer resistance of the electrode (R_{ct}) and the internal resistance (R_s),[28] respectively. R_{ct} is the diameter of the semicircle in the real part corresponding to the sum resistance of the electrochemical system, which is one of the limiting factors for the power densities of supercapacitors. Compared with PANI–GO and PANI–GO–MWNTs electrodes, the R_{ct} of the PANI–RGO–MWNTs electrode reduces remarkably due to the formation of a 3D conductive network by the use of MWNTs to bridge the gaps between the RGOs. The low resistance of the PANI–RGO–MWNTs electrode makes it possible for high-power performance flexible supercapacitors.

For further understanding of electrochemical performances, the long cycle life of the electrodes was also evaluated in our work by repeating the CV test at a scan rate of 50 mV s^{-1}. The specific capacitance as a function of the cycle number is

presented in Fig. 8d. It is found that the PANI–RGO–MWNTs electrode exhibits excellent long cycle life. After 3000 cycles, the capacitance retained 95.8% of the initial capacitance compared to 94.2% for the PANI–GO–MWNTs electrodes and 93.3% for the PANI–GO electrode. This demonstrates that the PANI–RGO–MWNTs electrode exhibits excellent cycle stability and a very high degree of reversibility in the repetitive scan cycle. The improved cycle stability is primarily attributed to the extraordinary electrical conductivity of the PANI–RGO–MWNTs electrode due to the formation of the 3D conductive network by introduction of MWNTs in the RGO system. Therefore, this ternary hybrid film has great potential application in flexible supercapacitors.

According to the abovementioned results of electrochemical performance, the good energy storage characteristics of the PANI–RGO–MWNTs flexible film are mainly attributed to two aspects. One is their special synergistic effect of three components, which combine the good redox property of PANI with high conductivity of MWNTs and RGO. Besides, the excellent performance of ternary hybrid film also depends on the novel 3D conductive network of the RGO bridging by MWNTs (Fig. 9). As is well known, GO after reduction is extremely defective compared to the high quality of graphene cleaved directly from graphite. Hence, the conductivity of RGO is far below the conductivity of graphene. In this paper, we successfully introduced MWNTs into the GO system, which effectively increased the basal spacing between GO sheets. More importantly, MWNTs were inserted into the layers of GO sheets, serving as a bridge to connect the defects induced by the reduction of GO (the defects in a single-layer graphene or adjacent layers). This is conducive for forming a 3D conductive network for efficient electron transfer, which endows rapid transport of the electrolyte ions and electrons throughout the electrode matrix, reducing the internal resistance of the electrode to result in the comprehensive utilization of pseudo-capacitance and double-layer capacitance. Thus, a high-performance ternary flexible supercapacitor can be obtained based on this 3D conductive network.

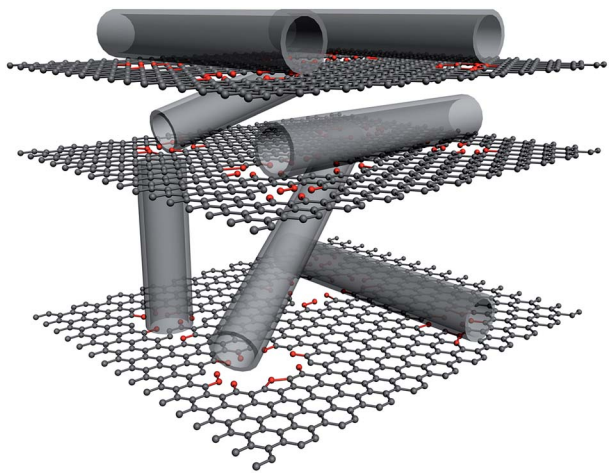

Fig. 9 Schematic representation of the superiority of the 3D conductive network using MWNTs to bridge the defect of the RGO for fast ion transport.

Conclusions

In summary, a 3D conductive network-supported free-standing PANI–RGO–MWNTs hybrid film has been designed and prepared by a simple rapid-mixture polymerization. The obtained ternary hybrid films maintain the pristine flexibility of GO–MWNTs film and display high electrochemical performances due to the remarkable combination of advantages due to the synergistic effect between MWNTs, RGO and PANI. More importantly, MWNTs serve as a bridge to connect the defects of RGO to form a 3D conductive network to enhance efficient electron transfer. Thus, a high-performance ternary flexible supercapacitor can be designed and prepared simply based on this 3D conductive network, making such film-like hybrid papers into promising flexible electrode materials for various applications in electrochemical energy storage such as flexible supercapacitors and batteries.

Acknowledgements

This work was supported by the National Natural Science Foundation of China (NSFC) (Grant no. 21121001), the Ministry of Science and Technology (2009CB930404) and the Shenzhen Science and Technology Research Grant (no. ZDSY20130331145131323, CXZZ20120829172325895, JCYJ 20120614150338154). We acknowledge Beijing Municipal Commission of Education for the special fund for the Disciplines & Postgraduate Education Construction Project.

Notes and references

1 M. Winter and R. J. Brodd, *Chem. Rev.*, 2004, **104**, 4245.
2 M. Armand and J. M. Tarascon, *Nature*, 2008, **451**, 652.
3 B. Kang and G. Ceder, *Nature*, 2009, **458**, 190.
4 H. J. Lin, L. Li, J. Ren, Z. B. Cai, L. B. Qiu, Z. B. Yang and H. S. Peng, *Sci. Rep.*, 2013, **3**, 1353.
5 Z. Niu, P. Luan, Q. Shao, H. Dong, J. Li, J. Chen, D. Zhao, L. Cai, W. Zhou, X. Chen and S. Xie, *Energy Environ. Sci.*, 2012, **5**, 8726.
6 D. W. Wang, F. Li, J. P. Zhao, W. C. Ren, Z. G. Chen, J. Tan, Z. S. Wu, I. Gentle, G. Q. Lu and H. M. Cheng, *ACS Nano*, 2009, **3**, 1745.
7 L. Ji, Z. Lin, A. J. Medford and X. Zhang, *Carbon*, 2009, **47**, 3346.
8 E. J. Ra, E. Raymundo-Piñero, Y. H. Lee and F. Béguin, *Carbon*, 2009, **47**, 2984.
9 X. Chen, L. Qiu, J. Ren, G. Guan, H. Lin, Z. Zhang, P. Chen, Y. Wang and H. Peng, *Adv. Mater.*, 2013, **25**, 6436.
10 J. Ren, W. Bai, G. Guan, Y. Zhang and H. Peng, *Adv. Mater.*, 2013, **25**, 5965.
11 Q. Wang, J. Yan, Z. Fan, T. Wei, M. Zhang and X. Jing, *J. Power Sources*, 2014, **247**, 197.
12 C. Meng, C. Liu, L. Chen, C. Hu and S. Fan, *Nano Lett.*, 2010, **10**, 4025.
13 L. Huang, B. Wu, G. Yu and Y. Liu, *J. Mater. Chem.*, 2011, **21**, 919.

14 C. Meng, C. Liu and S. Fan, *Electrochem. Commun.*, 2009, **11**, 186.
15 Q. Wu, Y. Xu, Z. Yao, A. Liu and G. Shi, *ACS Nano*, 2010, **4**, 1963.
16 L. L. Zhang, R. Zhou and X. S. Zhao, *J. Mater. Chem.*, 2010, **20**, 5983.
17 X. Fang, Z. Yang, L. Qiu, H. Sun, S. Pan, J. Deng, Y. Luo and H. Peng, *Adv. Mater.*, 2014, **26**, 1694.
18 Z. Yang, M. Liu, C. Zhang, W. W. Tjiu, T. Liu and H. Peng, *Angew. Chem., Int. Ed.*, 2013, **52**, 3996.
19 Z. Fan, J. Yan, L. Zhi, Q. Zhang, T. Wei, J. Feng, M. Zhang, W. Qian and F. Wei, *Adv. Mater.*, 2010, **22**, 3723.
20 N. I. Kovtyukhova, P. J. Ollivier, B. R. Martin, T. E. Mallouk, S. A. Chizhik, E. V. Buzaneva and A. D. Gorchinskiy, *Chem. Mater.*, 1999, **11**, 771.
21 S. Pei, J. Zhao, J. Du, W. Ren and H. M. Cheng, *Carbon*, 2010, **48**, 4466.
22 X. B. Yan, J. T. Chen, J. Yang, Q. J. Xue and P. Miele, *ACS Appl. Mater. Interfaces*, 2010, **2**, 2521.
23 R. V. Salvatierra, M. M. Oliveira and A. J. G. Zarbin, *Chem. Mater.*, 2010, **22**, 5222.
24 X. Lu, H. Dou, B. Gao, C. Yuan, S. Yang, L. Hao, L. Shen and X. Zhang, *Electrochim. Acta*, 2011, **56**, 5115.
25 J. Wei, J. Zhang, Y. Liu, G. Xu, Z. Chen and Q. Xu, *RSC Adv.*, 2013, **3**, 3957.
26 C. C. Hu and J. Y. Lin, *Electrochim. Acta*, 2002, **47**, 4055.
27 H. Fan, H. Wang, N. Zhao, X. Zhang and J. Xu, *J. Mater. Chem.*, 2012, **22**, 2774.
28 Y. Q. Dou, Y. P. Zhai, H. J. Liu, Y. Y. Xia, B. Tu, D. Y. Zhao and X. X. Liu, *J. Power Sources*, 2011, **196**, 1608.